energies

MDPI

Article

Low Temperature Aqueous Solution-Processed ZnO and Polyethylenimine Ethoxylated Cathode Buffer Bilayer for High Performance Flexible Inverted Organic Solar Cells

Hailong You [1], Junchi Zhang [1], Zeyulin Zhang [2], Chunfu Zhang [1,*], Zhenhua Lin [1,*], Jingjing Chang [1], Genquan Han [1], Jincheng Zhang [1], Gang Lu [3] and Yue Hao [1]

1 Wide Bandgap Semiconductor Technology Disciplines State Key Laboratory, School of Microelectronics, Xidian University, Xi'an 710071, China; hlyou@mail.xidian.edu.cn (H.Y.); chinasxhc@gmail.com (J.Z.); jjingchang@xidian.edu.cn (J.C.); gqhan@xidian.edu.cn (G.H.); jchzhang@xidian.edu.cn (J.Z.); yhao@xidian.edu.cn (Y.H.)

2 School of Textiles and Materials, Xi'an Polytechnic University, Xi'an 710048, China; zzylxg@sohu.com

3 Huanghe Hydropower Solar Industry Technology Co. Ltd., 369 South Yanta Road, Xi'an 710061, China; eelugang@163.com

* Correspondence: cfzhang@xidian.edu.cn (C.Z.); zhlin@xidian.edu.cn (Z.L.); Tel.: +86-29-882-017-59 (C.Z.); +86-29-882-048-89 (Z.L.)

Academic Editor: Claudia Barolo
Received: 19 February 2017; Accepted: 31 March 2017; Published: 6 April 2017

Abstract: High performance flexible inverted organic solar cells (OSCs) employing the low temperature cathode buffer bilayer combining the aqueous solution-processed ZnO and polyethylenimine ethoxylated (PEIE) are investigated based on Poly(3-hexylthiophene-2,5-diyl):[6,6]-phenyl-C_{61}-butyric acid methyl ester (P3HT:PC_{61}BM) and Poly({4,8-bis[(2-ethylhexyl)oxy]benzo[1,2-b:4,5-b′]dithiophene-2,6-diyl}{3-fluoro-2-[(2-ethylhexy)carbonyl]thieno[3,4-b]thiophenediyl}):[6,6]-phenyl-C_{71}-butyric acid methyl ester (PTB-7:PC_{71}BM) material systems. It is found that, compared with pure ZnO or PEIE cathode buffer layer (CBL), the proper combination of low-temperature processed ZnO and PEIE as the CBL enhanced the short circuit current density (J_{SC}), resulting in better device performance. The increased J_{SC} results from the enhanced electron collection ability from the active layer to the cathode. By using the ZnO/PEIE CBL, a power conversion efficiency (*PCE*) as high as 4.04% for the P3HT:PC_{61}BM flexible device and a *PCE* as high as 8.12% for the PTB-7:PC_{71}BM flexible device are achieved, which are higher than the control devices with the pure ZnO CBL or pure PEIE CBL. The flexible inverted OSC also shows a superior mechanical property and it can keep 92.9% of its initial performance after 1000 bending cycles with a radius of 0.8 cm. These results suggest that the combination of the low temperature aqueous solution processed ZnO and PEIE can be a promising cathode buffer bilayer for flexible inverted OSCs.

Keywords: organic solar cells (OSCs); cathode buffer layer (CBL); ZnO; polyethylenimine ethoxylated (PEIE)

1. Introduction

Due to the potential of low-cost, flexibility, light weight and compatibility with roll-to-roll fabrication, organic solar cells (OSCs) have attracted much research attention [1–4]. After continuous efforts in recent years, OSCs with power conversion efficiency (*PCE*) above 10%–12% have been achieved, based on the widely used bulk heterojunction (BHJ) of donor-accepter blend [5–7]. Generally, the structure of OSCs could be classified into two categories, namely conventional structure and

inverted structure. The conventional structure usually uses a poly(3,4-ethylenedioxithiophene): poly(styrenesulfonate) (PEDOT:PSS) hole transport layer on indium-tin-oxide (ITO) to collect holes and a low-work-function metal [aluminum (Al) or calcium (Ca)] top cathode to collect electrons. However, the acidic PEDOT:PSS layer can corrode the ITO electrode, leading to the indium diffusion into the active layer and resulting in interface instability [8–11]. And the top low-work-function metal can also be easily oxidized in air, resulting in poor stability [12–14]. Compared with the conventional structure, the inverted structure have the opposite electrode polarities, where the modified ITO acts as the cathode and a high-work-function metal such as silver (Ag) or gold (Au) acts as the top anode, so that both the commonly used acidic PEDOT:PSS and low-work-function metal top cathode can be avoided and morphology of the active layer become more stable. This structure has been considered as an efficient approach for improving the cell stability [15–19].

In inverted OSCs, an electron-selective layer between the ITO cathode and active layer is indispensable so that an ohmic contact for the decrease or elimination the electron-extraction barrier could be formed. N-type metal oxides such as zinc oxide (ZnO), titanium oxide (TiO_x), and tin oxide (SnO_2) have been introduced as a cathode buffer layer (CBL) to modify ITO as an effective electron-collecting electrode in inverted OSCs [1,2,15,20]. In particular, ZnO is more attractive because of its beneficial properties such as high electron mobility, high optical transparency, low-cost and simple solution process. Besides the metal oxides, polyelectrolyte such as polyethylenimine ethoxylated (PEIE) has also been widely used as CBL, which could also be processed by the simple solution processing method. PEIE contains simple aliphatic amine groups, which can produce surface dipoles and reduce the work function of the ITO electrode. Thus, the energy mismatch between the electrode and the active layer could be lowered so that the carriers can be efficiently collected by the electrode. The *PCE* of inverted OSCs with PEIE as CBL was comparable to inverted PSCs using ZnO as CBL. Recent reports [21,22] have shown that by combining ZnO and PEIE as the cathode buffer bilayer, the performance of OSCs could be further improved. However, in the reported cathode buffer bilayer, the deposition of ZnO is almost on the sol-gel method. This method usually requires a high process temperature (usually $\geq$300 °C), which is not compatible with flexible substrates such as polyethylene terephthalate (PET). Colloid-processed Nc-ZnO could be processed at a low temperature, but it possesses environmentally sensitive electrical performance in ambient atmosphere. In order to fabricate the flexible devices, the CBL combining a stable low temperature ZnO and PEIE should be developed.

Recent results [21,23–25] have shown that the aqueous solution of ammine-zinc complex is a promising technique to afford low temperature conversion to dense ZnO thin films. ZnO deposited using this method was first adopted to fabricate thin film transistor and later applied in organic light-emitting diodes and inverted OSCs. In particular, inverted OSCs based on ZnO CBL deposited by this method have showed efficient performance [20,23,24]. Ka et al. [25] and we [20,24] have shown that ZnO deposited by this aqueous solution could be processed at a low temperature so that most flexible substrates can withstand. In previously work [24], we have demonstrated that the *PCE* of flexible OSCs could reach 7.6% by using the aqueous solution processed ZnO as CBL. Besides, PEIE could be deposited at a low temperature (100 °C). This makes PEIE also very attractive for using in flexible devices. However, there is still no report about the cathode buffer bilayer combining the low temperature aqueous solution processed ZnO and PEIE used in flexible inverted OSCs.

In this work, we employed the low temperature cathode buffer bilayer combining the aqueous solution-processed ZnO and PEIE in flexible inverted OSCs based on Poly(3-hexylthiophene-2,5-diyl):[6,6]-phenyl-C_{61}-butryric acid methyl ester (P3HT:PC_{61}BM) and Poly({4,8-bis[(2-ethylhexyl)oxy] benzo[1,2-b:4,5-b′]dithiophene-2,6-diyl}{3-fluoro-2-[(2-ethylhexy)carbonyl]thieno[3,4-b]thiophenediyl}): [6,6]-phenyl-C_{71}-butyric acid methyl ester (PTB-7:PC_{71}BM). It is found that with proper combination of ZnO and PEIE as the CBL, the short circuit current density (J_{SC}) is obviously improved, resulting in better device performance compared with pure ZnO or PEIE CBL. The increased J_{SC} results from the enhanced electron collection ability from the active layer to the cathode. At the same time, the flexible

inverted OSCs showed a superior mechanical property. These results suggest that the combination of the low temperature aqueous solution processed ZnO and PEIE can be a promising cathode buffer bilayer for flexible inverted OSCs.

2. Results and Discussion

The schematic device structure of flexible inverted OSCs and the energy band diagram of the used materials are illustrated in Figure 1a,b. The inverted OSCs were fabricated on flexible PET substrates and with the structure of ITO/CBLs/P3HT:$PC_{61}BM$ or PTB7:$PC_{71}BM$/MoO_3/Ag. ZnO has conduction band energy of around −4.4 eV and valence band energy of around −7.8 eV, which suggests that electrons from the active layer can be transported into ZnO, while holes from the active layer can be blocked. At the same time, PEIE contains simple aliphatic amine groups and it can produce surface dipoles between the cathode and active layer. A very thin PEIE layer could reduce the work function of cathode and help the electron extraction. There are four different combinations of ZnO and PEIE for CBLs: pure ZnO, pure PEIE, ZnO/PEIE and PEIE/ZnO. Inverted OSCs based on the four different CBLs are fabricated.

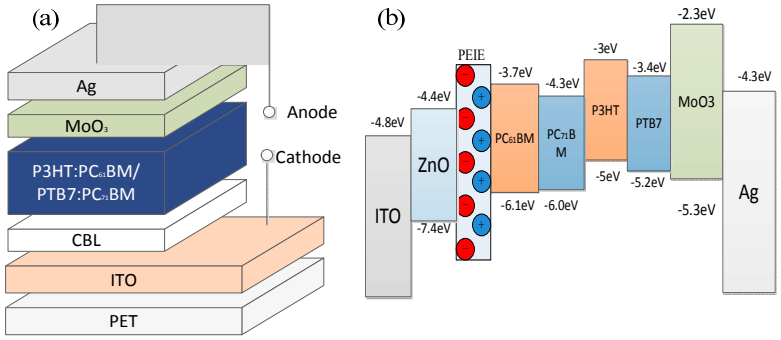

Figure 1. (**a**) The layer structure and (**b**) the corresponding energy band diagram of materials of the flexible organic solar cells (OSCs). P3HT:PC61BM: Poly(3-hexylthiophene-2,5-diyl):[6,6]-phenyl-C61-butryric acid methyl ester; PTB7:PC71BM: Poly({4,8-bis[(2-ethylhexyl)oxy]benzo[1,2-b:4,5-b′]dithiophene-2,6-diyl} {3-fluoro-2-[(2-ethylhexy)carbonyl]thieno[3,4-b]thiophenediyl}):[6,6]-phenyl-C_{71}-butyric acid methyl ester; CBL: cathode buffer layer; ITO: indium-tin-oxide; PET: polyethylene terephthalate; and PEIE: polyethylenimine ethoxylated.

The current density versus voltage (*J*-*V*) characteristics of the P3HT:$PC_{61}BM$ devices with different CBLs are shown in Figure 2a, and the extracted device parameters are summarized in Table 1. The parameters are extracted according to the Shockley equation:

$$J = J_0(\exp(\frac{q(V - R_s J)}{nk_B T}) - 1) + \frac{V - R_s J}{R_{sh}} - J_p \quad (1)$$

where J_0 is the saturation current, J_p the photocurrent, R_s the series resistance, R_{sh} the shunt resistance, n the ideality factor, q the electron charge, k_B the Boltzmann constant, and T the temperature. By using Equation (1) with our proposed explicit analytic expression method [26], the experimental data were extracted and these parameters could rebuild the *I*-*V* curves of the OSCs with different CBLs as shown in Figure 1a, which confirmed the validity of the extracted parameters. For the device with pure ZnO CBL, a J_{SC} of 9.16 mA/cm^2, an open circuit voltage (V_{OC}) of 0.65 V, and a fill factor (*FF*) of 63.61% are achieved which result in a *PCE* of 3.84%. The device with pure PEIE CBL shows a similar device performance with a *PCE* of 3.79%, a V_{OC} of 0.65 V, a J_{SC} of 9.19 mA/cm^2, and a *FF* of 62.87%. These results are comparable or even better compared to the reported OSCs with pure ZnO or PEIE CBL [24,27,28]. When we use PEIE/ZnO CBL in the device, a decreased device performance is obtained with a *PCE* of 3.12%, a V_{OC} of 0.64 V, a J_{SC} of 8.21 mA/cm^2, and a *FF* of 58.98%. Comparing

with the above OSCs, the device with ZnO/PEIE CBL exhibits the best performance as shown in Figure 2c,d, which obtains a *PCE* as high as 4.04%, with a J_{SC} of 9.81 mA/cm^2, a V_{OC} of 0.65 V, and a *FF* of 63.83%. The obviously increased J_{SC} should account for the performance improvement. To understand the improvement in the photovoltaic efficiency of the device with ZnO/PEIE CBL, the collected photocurrent (J_{ph}) as a function of effective voltage (V_{eff}), which reflects the internal field in the device, is plotted. J_{ph} is obtained by subtracting the current density in the dark from the current density under illumination. The V_{eff} is defined as $V_{eff} = V_o - V_a$, where V_o is the compensation voltage defined as the voltage where $J_{ph} = 0$ and V_a is the applied bias. As shown in Figure 2b, J_{ph} in the device with the ZnO/PEIE CBL is higher than in other devices from open-circuit condition to short-circuit condition. These results indicate that higher charge collection ability is achieved by the device with the ZnO/PEIE CBL, which is responsible for its higher *PCE*. The relatively low series resistance for the device with the ZnO/PEIE CBL also confirms that the ZnO/PEIE bilayer could further lower the energy barrier between the ITO electrode and the active layer, and then electron transport from the active layer to ITO is facilitated. This is the main reason for the higher J_{SC}.

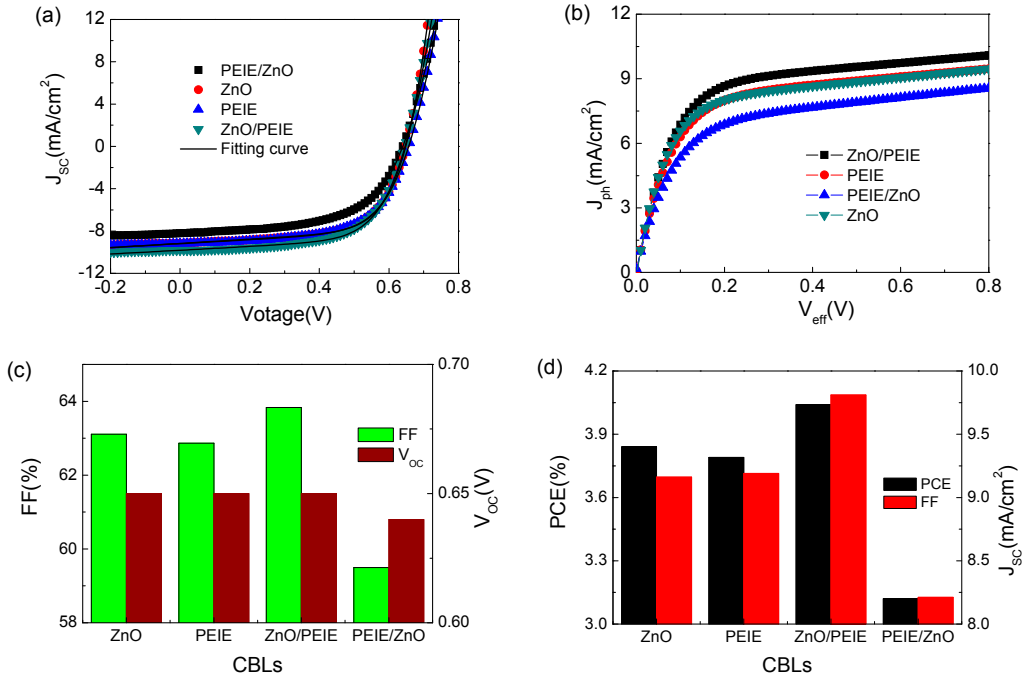

Figure 2. (**a**) The current density versus voltage (*J*-*V*) characteristics; (**b**) the collected photocurrent as a function of effective voltage (J_{ph}-V_{eff}) characteristics; (**c**) statistical chart of fill factor (*FF*) and open circuit voltage (V_{OC}); and (**d**) statistical chart of power conversion efficiency (*PCE*) and short circuit current density (J_{SC}) of the OSCs based on P3HT:PC_{61}BM with different CBLs.

Table 1. Photovoltaic performance parameters for flexible inverted P3HT:PC_{61}BM-based and PTB7:PC_{71}BM-based OSCs on PET.

Active Layer	CBLs	J_{SC} (mA/cm^2)	V_{OC} (V)	*FF* (%)	*PCE* (%)		R_s (Ω/cm^2)	R_{sh} (Ω/cm^2)
					Best	Ave		
P3HT:PC_{61}BM	ZnO	9.16	0.65	63.61	3.84	3.74	2.1	501.8
	PEIE	9.19	0.65	62.87	3.79	3.68	3.1	473.9
	ZnO/PEIE	9.81	0.65	63.83	4.04	3.93	2.7	479.7
	PEIE/ZnO	8.21	0.64	58.98	3.12	2.95	3.2	449.8
PTB-7:PC_{71}BM	ZnO	15.39	0.75	65.91	7.63	7.59	4.9	610.5
	PEIE	14.74	0.75	65.32	7.28	7.09	5.6	594.3
	ZnO/PEIE	16.48	0.75	66.01	8.12	8.00	4.1	645.1
	PEIE/ZnO	13.48	0.75	62.14	6.31	5.99	6.4	757.9

The four different CBLs were also applied to PTB-7:PC_{71}BM-based flexible inverted OSCs to test its feasibility in other material systems. Figure 3a shows the *J-V* curves and Table 1 shows the parameter summary of the flexible inverted PTB-7:PC_{71}BM OSCs. These devices show the same variation tendency of performance as that in the devices based on the P3HT:PC_{61}BM material system. The device with pure ZnO CBL achieves a *PCE* of 7.63% and with a V_{OC} of 0.75 V, a J_{SC} of 15.39 mA/cm^2 and a *FF* of 65.91%. And the device with pure PEIE CBL achieves a *PCE* of 7.28% with a V_{OC} of 0.75 V, a J_{SC} of 14.74 mA/cm^2 and a *FF* of 65.32%. Both of them have a comparable performance with the reported OSCs with pure ZnO or PEIE CBL [27–29]. And the lowest device performance is obtained when the PEIE/ZnO CBL is introduced. It only shows a *PCE* of 6.31% with a V_{OC} of 0.75 V, a J_{SC} of 13.48 mA/cm^2, and a *FF* of 62.14%. When we use ZnO/PEIE CBL, the highest device performance is obtained and a *PCE* as high as 8.12% is obtained with a V_{OC} of 0.75 V, a higher J_{SC} of 16.48 mA/cm^2, and a higher *FF* of 66.01%, as shown Figure 3b,c. These results demonstrate that the ZnO/PEIE bilayer could effectively enhance the performance of PTB-7:PC_{71}BM inverted OSCs and confirm its feasibility in different material systems.

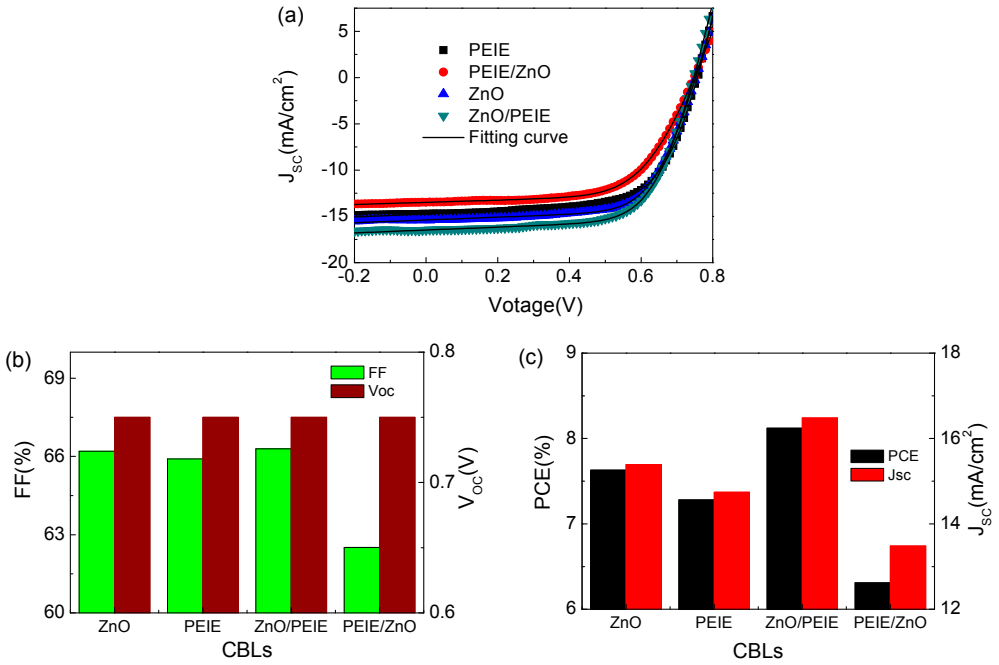

Figure 3. (**a**) *J-V* characteristics; (**b**) statistical chart of *FF* and V_{OC}, and (**c**) statistical chart of *PCE* and J_{SC} of the OSCs based on PTB-7:PC_{71}BM with different CBLs.

Figure 4 shows the statistical *PCE* of OSCs with different CBLs based on P3HT:PC_{61}BM and PTB-7:PC_{71}BM systems and the results show that the devices based on the ZnO/PEIE bilayer achieve a better performance, which confirms the validity of our above discussion. The incident photon-to-electron conversion efficiency (*IPCE)* spectra (SCS 100 IPCE system, Zolix instrument Co. Ltd., Beijing, China) of the OSCs devices with ZnO/PEIE CBL based on P3HT:PC_{61}BM and PTB7:PC_{71}BM are shown in Figure 5. The *IPCE* value approaches 68% around 550 nm for the device based on P3HT:PC_{61}BM. The J_{SC} calculated from integration of the *IPCE* spectrum from 300 nm to 800 nm is 9.64 mA/cm^2. For the device based on PTB-7:PC_{71}BM, the *IPCE* value approaches 77% around 600 nm. The J_{SC} calculated from integration of the *IPCE* spectrum from 300 nm to 800 nm is 16.14 mA/cm^2. The calculated J_{SC} is near the values obtained from the *I-V* measurements.

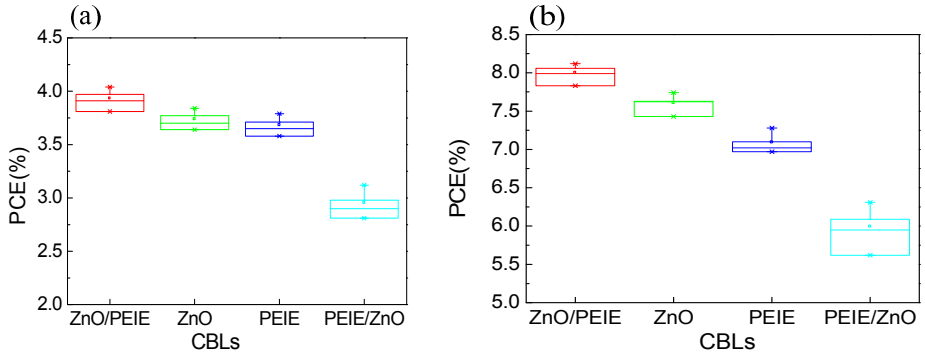

Figure 4. Performance statistical results of OSCs with different CBLs based on (**a**) P3HT:PC_{61}BM and (**b**) PTB-7:PC_{71}BM.

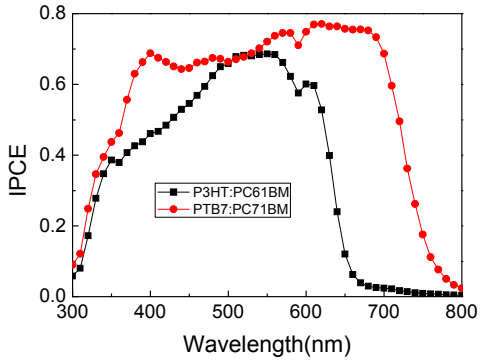

Figure 5. Incident photon-to-electron conversion efficiency (*IPCE*) spectra of the OSCs devices with ZnO/PEIE CBL based on P3HT:PC_{61}BM and PTB-7:PC_{71}BM.

It can be seen from Figures 2 and 3, the lowest device performance is obtained for the OSC with the PEIE/ZnO CBL. The combination of ZnO and PEIE in this configuration leads to the negative effects on the J_{SC} and FF. In fact, the obvious transmittance difference between the PEIE/ZnO sample and other samples can be distinguished by eyes in the experiments. To investigate the optical property differences of the four different CBL films, the ultra violet visible (UV-Vis) wavelength optical transmittance spectra (LAMBDA-950, PERKIN-ELMER, Waltham, MA, USA) of the films with pure ZnO, pure PEIE, ZnO/PEIE, and PEIE/ZnO CBLs were measured and shown in Figure 6. As can be seen, all the samples with the configurations of pure ZnO, pure PEIE, and ZnO/PEIE have good transmittances in the visible wavelength range. These results indicate that the ZnO interlayer, PEIE interlayer and ZnO/PEIE interlayer have minimal effect on the light absorption of active layer. However, there is obviously lower light transmittance for the sample with the configuration of PEIE/ZnO at wavelength from 400 nm to 700 nm. The lower light transmittance of PEIE/ZnO film in the visible wavelength range would result in a lower J_{SC} in the corresponding OSC. This must be one important reason for the inferior performance of device with PEIE/ZnO CBL. One possible explanation is that PEIE could be dissolved in water and the used ZnO is deposited by an aqueous solution method. During the deposition of the ZnO precursor, the aqueous solution of ammine-zinc complex may destroy the underlined PEIE film and then results in the lower light transmittance. In order to verify our hypothesis, we take optical microscopy images of the four CBLs. The optical microscopy images of ITO/ZnO, ITO/ZnO/PEIE, ITO/PEIE/ZnO, and ITO/ZnO are presented in Figure 7. It can be seen in the optical microscopy image of ITO/PEIE/ZnO that there are many winkles or cracks in this sample, which is obviously different from other samples where the surface is rather smooth. This confirms our hypothesis that the deposition of ZnO destroys the underlying PEIE film.

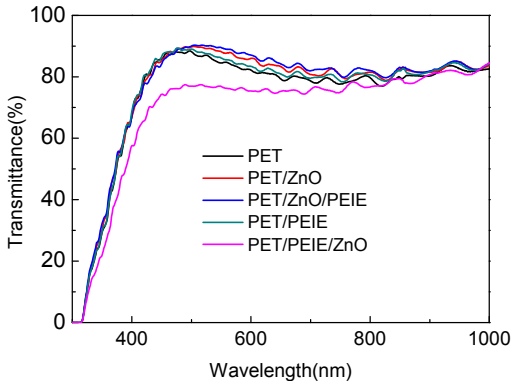

Figure 6. Transmittance spectra of the films with ZnO, ZnO/PEIE, PEIE, PEIE/ZnO CBL.

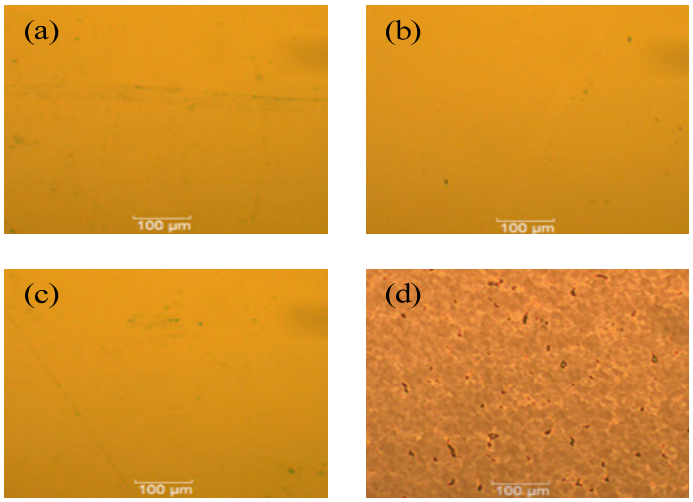

Figure 7. The optical microscopy images of (**a**) PET/ITO/ZnO; (**b**) PET/ITO/PEIE; (**c**) PET/ITO/ZnO/PEIE; and (**d**) PET/ITO/PEIE/ZnO. The particles in (**a**–**c**) are used for focus to make the optical microscopy images clear.

To further investigate the surface characteristic of CBLs, an atomic force microscope (AFM) (Agilent 5500, Agilent Technologies, Palo Alto, CA, USA) was adopted to measure the surface morphology of ITO/ZnO, ITO/ZnO/PEIE, ITO/PEIE/ZnO, and ITO/ZnO. The measurement results are illustrated in Figure 8. The root mean square (*RMS*) roughness was 1.3 nm, 1.5 nm, 2.1 nm, and 10.5 nm for the samples with the configuration of PEIE, ZnO/PEIE, ZnO, and PEIE/ZnO, respectively. The *RMS* value (10.5 nm) of PEIE/ZnO is far larger than other three RMS values of ZnO (2.1 nm), ZnO/PEIE (1.5 nm), and PEIE (1.3 nm). The rough surface of PEIE/ZnO suggests that the PEIE film is destroyed by the following ZnO deposition, which is consistent with the transmittance and optical microscopy measurements. On the other hand, by capping PEIE on ZnO, a smaller RMS value (1.5 nm) of ZnO/PEIE is achieved compared with that of ZnO (2.1 nm). This means that there is a smoother surface for the sample of ZnO/PEIE compared to the pure ZnO and the smoother morphology supplies excellent contact between the active layer and CBL, which is consistent with the better device performance.

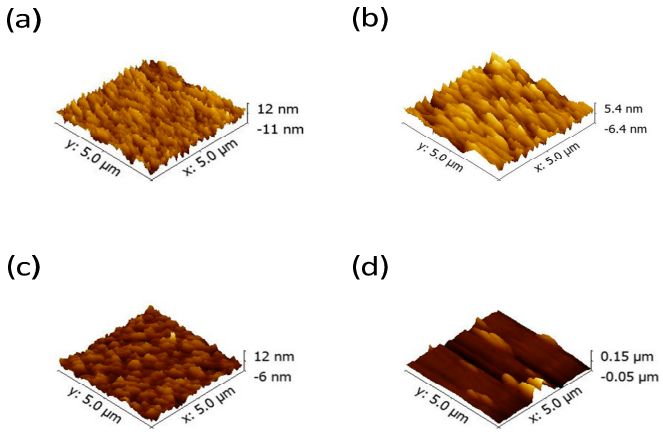

Figure 8. Surface morphology of (**a**) ZnO; (**b**) PEIE; (**c**) ZnO/PEIE; and (**d**) PEIE/ZnO.

Another possible reason for the different J_{SC} values is that the effects of the different surface energy of CBLs on the active layer formation. To study the influence of different CBLs on the active layer, we carried out a contact angle measurement of the CBL films. The consequence of water contact angle measurement is displayed in Figure 9. As illustrated in Figure 9, due to application of UV ozone treatment, all of the four different CBLs show good hydrophilicity. The contact angles of 16.8° (ZnO), 18.1° (PEIE), 17.7° (ZnO/PEIE), and 21.2° (PEIE/ZnO) were very close. The delicate difference would not cause much impact on film formation of active layer. This indicated the influence caused by hydrophilicity of CBL on thickness could be neglected.

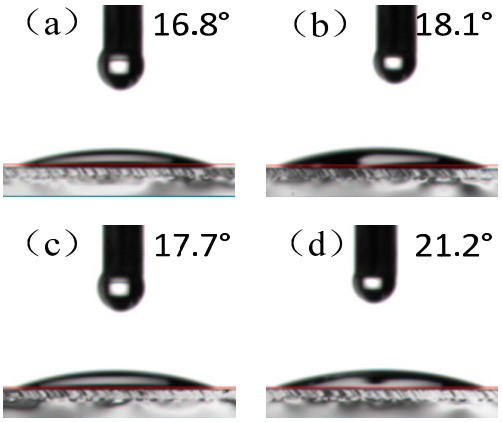

Figure 9. The water contact angle of OSC devices with (**a**) ZnO CBL; (**b**) PEIE CBL; (**c**) PEIE/ZnO CBL; and (**d**) ZnO/PEIE CBL.

The flexibility property of OSCs with different CBLs (pure ZnO, pure PEIE, ZnO/PEIE, and PEIE/ZnO) based on PTB-7:$PC_{71}BM$ material system was also studied. The consequence of bending test is illustrated in Figure 10. It can be seen that all of OSCs with pure ZnO CBL, pure PEIE CBL, and ZnO/PEIE CBL show similar flexibility property. After 1000 bending cycles with a radius of 0.8 cm, OSCs with pure ZnO CBL, pure PEIE CBL, and ZnO/PEIE CBL could keep 90.5%, 93.0%, and 92.9% of their initial performance, respectively. However, the *PCE* of OSC with PEIE/ZnO CBL, which is also the device with lowest *PCE*, decreases quickly in the bending test and only keeps by 80% of its original value after 1000 bending cycles. The inferior characteristic of PEIE/ZnO film affects not only the device performance but also the flexibility property of OSCs.

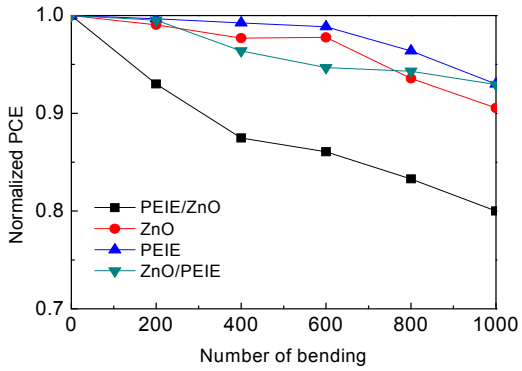

Figure 10. Normalized device *PCE* as a function of the number of bending cycles with a radius of 0.8.

3. Materials and Methods

3.1. Preparation of Materials

For the ZnO precursor solution, ZnO aqueous solution was prepared by dissolving 10 mg ZnO powder in 1 mL ammonia to form 0.125 M $Zn(NH_3)_4^{2+}$ solution. Then the solution was ultrasonically processed for 5–10 min and stored in refrigerator at 0–10 °C for more than 12 h before use. For PEIE solution, PEIE was dissolved in 2-methoxy ethanol to form 0.2 wt% PEIE solutions. The solutions were then stirred for 12 h at room temperature before use.

For P3HT:PC_{61}BM, a mixture of P3HT and PC_{61}BM at a weight ratio of 1:0.8 was dissolved in 1,2-dichlorobenzene(1,2-DCB) and then put on the heating stage stirred for more than 12 h. For PTB-7:PC_{71}BM, a mixture of PTB-7:PC_{71}BM at a weight ratio of 1:1.5 was dissolved in dichlorobenzene (CB). Then, 1,8-diiodooctane (DIO) was added to the solution at a concentration of 3 vol%. Finally, just like the preparation process of P3HT:PC_{61}BM, the solution was also stirred for more than 12 h.

The ITO-coated PET substrates were supplied by Zhuhai Kaivo (Zhuhai, China). PCBM and DIO were purchased from Nano-C (Westwood, MA, USA) and Alfa (Heysham, UK), respectively. PTB7 and P3HT were provided by 1-materials (Dorval, QC, Canada) and Rieke Metals (Lincoin, NE, USA,). ZnO, CB, 1,2-DCB, and MoO_3 were supplied by Sigma Aldrich (St. Louis, MO, USA).

3.2. Fabrication and Measurement of Flexible Organic Solar Cells

The devices were fabricated with a structure of ITO/CBLs/active layer/MoO_3/Ag as in Figure 1a, in which CBLs are pure ZnO, pure PEIE, ZnO/PEIE, or PEIE/ZnO, and the active layer are P3HT:PC_{61}BM or PTB-7:PC_{71}BM films. Figure 1 shows the layer structure of the device. The fabrication processes were as follows: ITO-coated PET substrates were sequentially cleaned with detergent, deionized water, and ethanol in an ultrasonic bath for 20 min, and then were blow-dried with a nitrogen gun. Then, UV ozone was applied to the ITO surface for 30 min. The ZnO aqueous solution was spin-cast on the cleaned ITO-PET substrate at 3000 rpm for 40 s, and then annealed in the oven at 150 °C for 30 min. The PEIE layer was deposited via spin-coating method at 5000 RPM for 60 s and followed by annealing at 100 °C in the oven too. The polymer solution was then spun-casted on the CBL at 1000 RPM for 60 s for PTB7:PC_{71}BM or at 800 RPM for 120 s for P3HT:PC_{61}BM in glove box, respectively. After the films were slow dried in glove box for 3 h, the P3HT-based devices should be extra pre-annealed on a heating stage at 150 °C for 10 min. Then 10 nm MoO_3 and 80 nm Ag were thermally evaporated onto the active layer through a metal shadow mask. The devices' area was about 8 mm^2

The *J-V* characteristics of the devices were measured by a Xenon lamp (XEC-300M2, SANEI ELECTRIC, Shizuoka, Japan) with an air mass (AM) 1.5 G filteratan intensity of 100 mW/cm^2 and a Keithley 2400 source-measure unit [30]. The Xenon lamp is verified through a standard

Si solar cell calibrated by the National Renewable Energy Laboratory (NREL). The transmittance spectra of the PET/ITO/ZnO, PET/ITO/PEIE, PET/ITO/ZnO/PEIE, and PET/ITO/PEIE/ZnO were measured by a UV/Vis/NIR spectrophotometer (LAMBDA-950, PERKIN-ELMER, Waltham, MA, USA). The surface optical morphology of PET/ITO/ZnO, PET/ITO/PEIE, PET/ITO/ZnO/PEIE, and PET/ITO/PEIE/ZnO was investigated by the Leica DM4000M optical microscopy (Wetzlar, Germany). Tapping mode AFM tests were performed to test the thin films morphology by an Agilent 5500 scanning probe system (Agilent 5500, Agilent Technologies, Palo Alto, CA, USA). The water contact angle measurement was carried out by a contact angle meter (JC2000DM, Beijing Zhongyikexin Science and Technology Co. Ltd., Beijing, China).

4. Conclusions

In summary, we have fabricated and investigated high performance flexible inverted OSCs by employing low temperature aqueous solution processed ZnO and PEIE bilayer film with high transparency and good electron transporting properties as the CBL. By using the ZnO/PEIE CBL, the highest *PCE* of 4.04%, based on P3HT:PC_{61}BM, and 8.12%, based on PTB-7:PC_{71}BM, are achieved, which are higher than the control device with the pure ZnO CBL or pure PEIE CBL. Meanwhile, the inverted OSC also shows superior flexibility and it can keep 92.9% of its initial performance after 1000 bending cycles with a radius of 0.8 cm. This study indicates that the low-temperature solution-processed ZnO/PEIE bilayer significantly enhanced charge collection efficiency which is beneficial for high performance inverted OSCs and suitable for flexible devices.

Acknowledgments: This study was partly financially supported by National Natural Science Foundation of China (61334002, 61106063, 61534004, 61604119) and the Fundamental Research Funds for the Central Universities (JB151406, JB161101, JB161102).

Author Contributions: Chunfu Zhang and Zhenhua Lin conceived the idea and guided the experiment, Hailong You and Junchi Zhang conducted most of device fabrication, data collection. Chunfu Zhang wrote the manuscript, Zhenhua Lin and Jingjing Chang revised the manuscript, Zeyulin Zhang, Genquan Han, Jincheng Zhang, Gang Lu helped the device measurement, and Yue Hao supervised the team. All authors read and approved the manuscript.

Conflicts of Interest: The authors declare no conflicts of interest.

References

1. Baek, W.H.; Seo, I.; Yoon, T.S.; Lee, H.H.; Yun, C.M.; Kim, Y.S. Hybrid inverted bulk heterojunction solar cells with nanoimprinted TiO_2 nanopores. *Sol. Energy Mater. Sol. Cells* **2009**, *93*, 1587–1591. [CrossRef]
2. Wang, J.C.; Weng, W.T.; Tsai, M.Y.; Lee, M.K.; Horng, S.F.; Perng, T.P.; Kei, C.C.; Yu, C.C.; Meng, H.F. Highly efficient flexible inverted organic solar cells using atomic layer deposited ZnO as electron selective layer. *J. Mater. Chem.* **2010**, *20*, 862–866. [CrossRef]
3. Zhang, F.; Xu, X.; Tang, W.; Zhang, J.; Zhuo, Z.; Wang, J.; Wang, J.; Xu, Z.; Wang, Y. Recent development of the inverted configureuration organic solar cells. *Sol. Energy Mater. Sol. Cells* **2011**, *95*, 1785–1799. [CrossRef]
4. Huang, J.S.; Chou, C.Y.; Liu, M.Y.; Tsai, K.H.; Lin, W.H.; Lin, C.F. Solution-processed vanadium oxide as an anode interlayer for inverted polymer solar cells hybridized with ZnO nanorods. *Org. Electron.* **2009**, *10*, 1060–1065. [CrossRef]
5. Ye, L.; Zhao, W.; Li, S.; Mukherjee, S.; Carpenter, J.H.; Awartani, O.; Jiao, X.; Hou, J.; Ade, H. High-efficiency nonfullerene organic solar cells: Critical factors that affect complex multi-length scale morphology and device performance. *Adv. Energy Mater.* **2016**. [CrossRef]
6. Zhang, S.; Ye, L.; Hou, J. Breaking the 10% efficiency barrier in organic photovoltaics: Morphology and Device optimization of well-known PBDTTT polymers. *Adv. Energy Mater.* **2016**, *6*, 1502529. [CrossRef]
7. Huang, J.; Li, C.Z.; Chueh, C.C.; Liu, S.Q.; Yu, J.S.; Jen, A.K.Y. 10.4% Power conversion efficiency of ITO-free organic photovoltaics through enhanced light trapping configureuration. *Adv. Energy Mater.* **2015**, *5*. [CrossRef]
8. Jørgensen, M.; Norrman, K.; Gevorgyan, S.A.; Tromholt, T.; Andreasen, B.; Krebs, F.C. Stability of polymer solar cells. *Adv. Mater.* **2012**, *24*, 580–612. [CrossRef] [PubMed]

9. Min, J.; Luponosov, Y.N.; Zhang, Z.G.; Ponomarenko, S.A.; Ameri, T.; Li, Y.; Brabec, C.J. Interface design to improve the performance and stability of solution-processed small-molecule conventional solar cells. *Adv. Energy Mater.* **2014**, *4*, 1400816. [CrossRef]
10. Chen, D.; Zhang, C.; Heng, T.; Wei, W.; Wang, Z.; Han, G.; Feng, Q.; Hao, Y.; Zhang, J. Efficient inverted polymer solar cells using low-temperature zinc oxide interlayer processed from aqueous solution. *Jpn. J. Appl. Phys.* **2015**, *54*, 042301. [CrossRef]
11. Savagatrup, S.; Printz, A.D.; O'Connor, T.F.; Zaretski, A.V.; Rodriquez, D.; Sawyer, E.J.; Rajan, K.M.; Acosta, R.I.; Root, S.E.; Lipomi, D.J. Mechanical degradation and stability of organic solar cells: Molecular and microstructural determinants. *Energy Environ. Sci.* **2015**, *8*, 55–80. [CrossRef]
12. Pachoumi, O.; Li, C.; Vaynzof, Y.; Bange, K.K.; Sirrintghaus, H. Improved performance and stability of inverted organic solar cells with sol-gel processed, amorphous mixed metal oxide electron extraction layers comprising alkaline earth metals. *Adv. Energy Mater.* **2013**, *3*, 1428–1436. [CrossRef]
13. Chen, D.; Zhang, C.; Wei, W.; Wang, Z.; Heng, T.; Tang, S.; Han, G.; Zhang, J.; Hao, Y. Stability of inverted organic solar cells with low—Temperature ZnO buffer layer processed from aqueous solution. *Phys. Status Solidi A* **2015**, *212*, 2262–2270. [CrossRef]
14. Zhang, C.; You, H.; Lin, Z.; Hao, Y. Inverted organic photovoltaic cells with solution-processed zinc oxide as electron collecting layer. *Jpn. J. Appl. Phys.* **2011**, *50*, 082302. [CrossRef]
15. Lin, Z.; Jiang, C.; Zhu, C.; Zhang, J. Development of inverted organic solar cells with TiO_2 interface layer by using low-temperature atomic layer deposition. *ACS. Appl. Mater. Interfaces* **2013**, *5*, 713–718. [CrossRef] [PubMed]
16. Lin, Z.; Chang, J.; Zhang, J.; Jiang, C.; Wu, J.; Zhu, C. A work-function tunable polyelectrolyte complex (PEI:PSS) as a cathode interfacial layer for inverted organic solar cells. *J. Mater. Chem. A.* **2014**, *2*, 7788–7794. [CrossRef]
17. Chang, J.; Lin, Z.; Jiang, C.; Zhang, J.; Zhu, C.; Wu, J. Improve the operational stability of the inverted organic solar cells using bilayer metal oxide structure. *ACS Appl. Mater. Interfaces* **2014**, *6*, 18861–18867. [CrossRef] [PubMed]
18. Wang, W.; Schaffer, C.J.; Song, L.; Körstgens, V.; Pröller, S.; Indari, E.D.; Wang, T.; Abdelsamie, A.; Bernstorff, S.; Müller-Buschbaum, P. In operando morphology investigation of inverted bulk heterojunction organic solar cells by GISAXS. *J. Mater. Chem. A* **2015**, *3*, 8324–8331. [CrossRef]
19. Wang, W.; Pröller, S.; Niedermeier, M.A.; Körstgens, V.; Philipp, M.; Su, B.; González, D.M.; Yu, S.; Roth, S.V.; Müller-Buschbaum, P. Development of the morphology during functional stack build-up of P3HT:PCBM bulk heterojunction solar cells with inverted geometry. *ACS. Appl. Mater. Interfaces* **2014**, *7*, 602–610. [CrossRef] [PubMed]
20. Wei, W.; Zhang, C.; Chen, D.; Wang, Z.; Zhu, C.; Zhang, J.; Lu, X.; Hao, Y. Efficient "light-soaking"-free inverted organic solar cells with aqueous solution processed low-temperature zno electron extraction layers. *ACS. Appl. Mater. Interfaces* **2013**, *5*, 13318–13324. [CrossRef] [PubMed]
21. Li, P.; Cai, L.; Wang, G.; Xiang, J.; Zhang, Y.J.; Ding, B.F.; Alameh, K.; Song, Q.L. PEIE capped ZnO as cathode buffer layer with enhanced charge transfer ability for high efficiency polymer solar cells. *Synthet. Met.* **2015**, *203*, 243–248. [CrossRef]
22. Courtright, B.A.E.; Jenekhe, S.A. Polyethylenimine interfacial layers in inverted organic photovoltaic devices: Effects of ethoxylation and molecular weight on efficiency and temporal stability. *ACS. Appl. Mater. Interfaces* **2015**, *7*, 26167–26175. [CrossRef] [PubMed]
23. Bai, S.; Wu, Z.; Xu, X.; Jin, Y.; Sun, B.; Guo, X.; He, S.; Wang, X.; Ye, Z.; Wei, H.; et al. Inverted organic solar cells based on aqueous processed ZnO interlayers at low temperature. *Appl. Phys. Lett.* **2012**, *100*, 203906. [CrossRef]
24. You, H.; Zhang, J.; Zhang, C.; Lin, Z.; Chen, D.; Chang, J.; Zhang, J. Efficient flexible inverted small-bandgap organic solar cells with low-temperature zinc oxide interlayer. *Jpn. J. Appl. Phys.* **2016**, *55*, 122302. [CrossRef]
25. Ka, Y.; Lee, E.; Park, S.Y.; Seo, J.; Kwon, D.G.; Lee, H.H.; Park, Y.; Kim, Y.S.; Kim, C. Effects of annealing temperature of aqueous solution-processed ZnO electron-selective layers on inverted polymer solar cells. *Org. Electron.* **2013**, *14*, 100–104. [CrossRef]
26. Zhang, C.; Zhang, J.; Hao, Y.; Lin, Z.; Zhu, C. A simple and efficient solar cell parameter extraction method from a single current-voltage curve. *J. Appl. Phys.* **2011**, *110*, 064504. [CrossRef]

27. Li, P.; Wang, G.; Cai, L.; Ding, B.; Zhou, D.; Hu, Y.; Zhang, Y.; Xiang, J.; Wan, K.; Chen, L.; et al. High-efficiency inverted polymer solar cells controlled by the thickness of polyethylenimine ethoxylated (PEIE) interfacial layers. *Phys. Chem. Chem. Phys.* **2014**, *16*, 23792–23799. [CrossRef] [PubMed]
28. Hu, T.; Li, L.; Xiao, S.; Yuan, K.; Yang, H.; Chen, L.; Chen, Y. In situ implanting carbon nanotube-gold nanoparticles into ZnO as efficient nanohybrid cathode buffer layer for polymer solar cells. *Org. Electron.* **2016**, *38*, 350–356. [CrossRef]
29. Lee, T.H.; Choi, H.; Walker, B.; Kim, T.; Kim, H.B.; Kim, J.Y. Replacing the metal oxide layer with a polymer surface modifier for high-performance inverted polymer solar cells. *RSC. Adv.* **2014**, *4*, 4791–4795. [CrossRef]
30. Ye, L.; Zhou, C.; Meng, H.; Wu, H.H.; Lin, C.C.; Liao, H.H.; Zhang, S.; Hou, J. Toward reliable and accurate evaluation of polymer solar cells based on low band gap polymers. *J. Mater. Chem.* **2015**, *3*, 564–569. [CrossRef]

© 2017 by the authors. Licensee MDPI, Basel, Switzerland. This article is an open access article distributed under the terms and conditions of the Creative Commons Attribution (CC BY) license (http://creativecommons.org/licenses/by/4.0/).